Supplementary Material for "Disentangling uncertainty in ISMIP6 Antarctic sub-shelf melting and 2300 sea level rise projections"

Johanna Beckmann[1], Ronja Reese[2], Felicity S. McCormack[1], Sue Cook[3], Lawrence Bird[1], David Gwyther[4], Daniel Richards[5,6], Matthias Scheiter[5], Yu Wang[3], Hélène Seroussi[7], Ayako Abe-Ouchi[8], Torsten Albrecht[9,10], Jorge Alvarez-Solas[11,12], Xylar S. Asay-Davis[13], Jean-Baptiste Barre[14], Constantijn J. Berends[15], Jorge Bernales[15], Javier Blasco[16], Justine Caillet[17,7], David M. Chandler[18], Violaine Coulon[19], Richard Cullather[20], Christophe Dumas[21], Benjamin K. Galton-Fenzi[3,22], Julius Garbe[9,23], Fabien Gillet-Chaulet[17], Rupert Gladstone[24], Heiko Goelzer[18], Nicholas R. Golledge[25], Ralf Greve[26,27], G. Hilmar Gudmundsson[2], Holly Kyeore Han[13,28], Trevor R. Hillebrand[13], Matthew J. Hoffman[13], Philippe Huybrechts[29], Nicolas C. Jourdain[17], Ann Kristin Klose[9,23], Petra M. Langebroek[18], Gunter R. Leguy[30], William H. Lipscomb[30], Daniel P. Lowry[31], Pierre Mathiot[17], Marisa Montoya[11,12], Mathieu Morlighem[32], Sophie Nowicki[33], Frank Pattyn[19], Antony J. Payne[34], Tyler Pelle[35], Aurélien Quiquet[21], Alexander Robinson[11,16], Leopekka Saraste[36], Erika G. Simon[20], Sainan Sun[2], Jake P. Twarog[7], Luke D. Trusel[37], Benoit Urruty[17], Jonas Van Breedam[29], Roderik S. W. van de Wal[15,38,39], Chen Zhao[3], and Thomas Zwinger[36]

[1]Securing Antarctica's Environmental Future, School of Earth, Atmosphere & Environment, Monash University, Clayton, Kulin Nations, Victoria, Australia
[2]Northumbria University, Newcastle, UK
[3]Australian Antarctic Program Partnership, Institute for Marine and Antarctic Studies, University of Tasmania, Nipaluna / Hobart, Lutruwita / Tasmania, Australia
[4]School of Earth and Environmental Sciences, The University of Queensland, St Lucia, Queensland, Australia
[5]Australian Centre for Excellence in Antarctic Science, Institute for Marine and Antarctic Studies, and School of Natural Sciences (Physics), University of Tasmania, Nipaluna / Hobart, Lutruwita / Tasmania, Australia
[6]British Antarctic Survey, Cambridge, England, UK
[7]Thayer School of Engineering, Dartmouth College, Hanover, NH, USA
[8]Atmosphere and Ocean Research Institute, University of Tokyo, Kashiwa, Japan
[9]Potsdam Institute for Climate Impact Research (PIK), Member of the Leibniz Association, Potsdam, Germany
[10] Department of Integrative Earth System Science, Max Planck Institute of Geoanthropology, Kahlaische Str. 10, 07745 Jena, Germany
[11]Departamento de Física de la Tierra y Astrofísica, Facultad de Ciencias Físicas, Universidad Complutense de Madrid, Madrid, Spain
[12]Instituto de Geociencias, Consejo Superior de Investigaciones Científicas, Universidad Complutense de Madrid, Madrid, Spain
[13]Fluid Dynamics and Solid Mechanics Group, Los Alamos National Laboratory, Los Alamos, NM, USA
[14]Department of Earth System Science, University of California Irvine, Irvine, CA, USA
[15]Institute for Marine and Atmospheric Research Utrecht, Utrecht University, Utrecht, The Netherlands
[16]Alfred Wegener Institute, Helmholtz Centre for Polar and Marine Research, Potsdam, Germany
[17]Univ. Grenoble Alpes/CNRS/INRAE/IRD/G-INP, Institut des Géosciences de l'Environnement, Grenoble, France
[18]NORCE Norwegian Research Centre, Bjerknes Centre for Climate Research, Bergen, Norway
[19]Laboratoire de Glaciologie, Université libre de Bruxelles, Brussels, Belgium
[20]NASA Goddard Space Flight Center, Greenbelt, MD, USA

[21]Laboratoire des Sciences du Climat et de l'environnement, LSCE-IPSL, CEA-CNRS-UVSQ, Université Paris-Saclay, Paris, France
[22]Australian Antarctic Division, Kingston, Tasmania, Australia
[23]Institute of Physics and Astronomy, University of Potsdam, Potsdam, Germany
[24]Arctic Centre, University of Lapland, Rovaniemi, Finland
[25]Antarctic Research Centre, Victoria University of Wellington, Wellington, New Zealand
[26]Institute of Low Temperature Science, Hokkaido University, Sapporo, Japan
[27]Arctic Research Center, Hokkaido University, Sapporo, Japan
[28]Earth Surface and Interior Group, Jet Propulsion Laboratory, Pasadena, CA, USA
[29]Earth System Science & Departement Geografie, Vrije Universiteit Brussel, Brussels, Belgium
[30]Climate and Global Dynamics Laboratory, NSF National Center for Atmospheric Research, Boulder, CO, USA
[31]GNS Science, Lower Hutt, New Zealand
[32]Department of Earth Sciences, Dartmouth College, Hanover, NH, USA
[33]Department of Geology, University at Buffalo, Buffalo, NY, USA
[34]University of Liverpool, Liverpool, UK
[35]Scripps Institution of Oceanography, University of California San Diego, La Jolla, CA, USA
[36]CSC-IT Center for Science, Espoo, Finland
[37]Department of Geography, Pennsylvania State University, University Park, PA, USA
[38]Department of Physical Geography, Utrecht University, Utrecht, The Netherlands
[39]The Royal Netherlands Meteorological Institute, De Bilt, The Netherlands

Correspondence: Johanna Beckmann (johanna.beckmann@monash.edu)

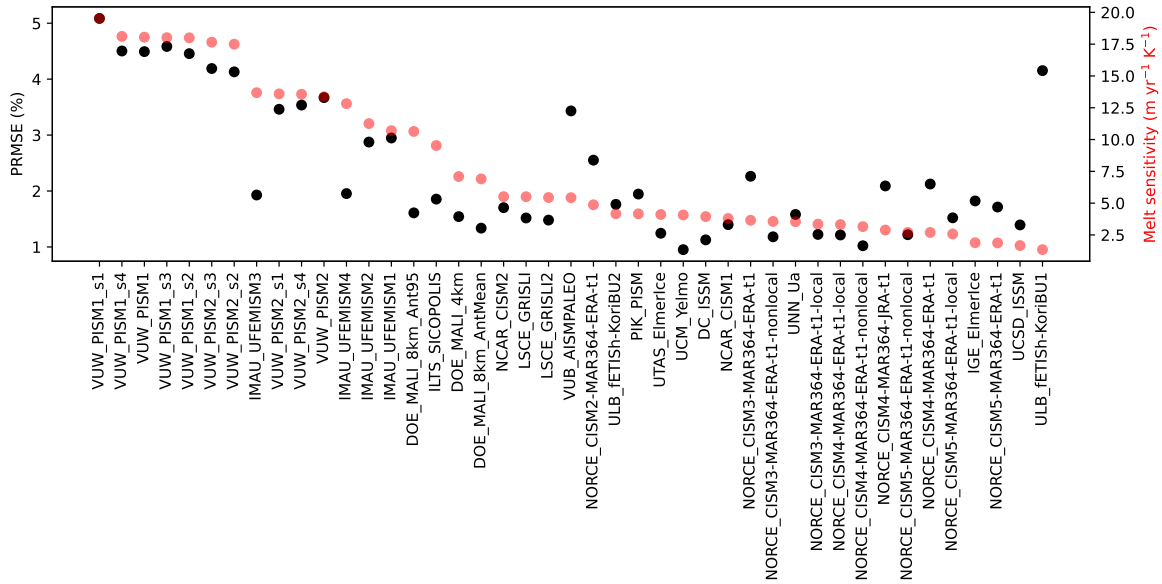

Figure S1. Percentage root mean square error (PRMSE; %) between the actual and predicted basal melt (black) for the aggregated AIS data, and the corresponding melt sensitivity factors ($\mathrm{m\,yr^{-1}\,K^{-1}}$; red). PRMSEs are averaged over the four climate experiments. The lowest PRMSE of the three fitting methods tested is shown for each ice sheet model simulation.

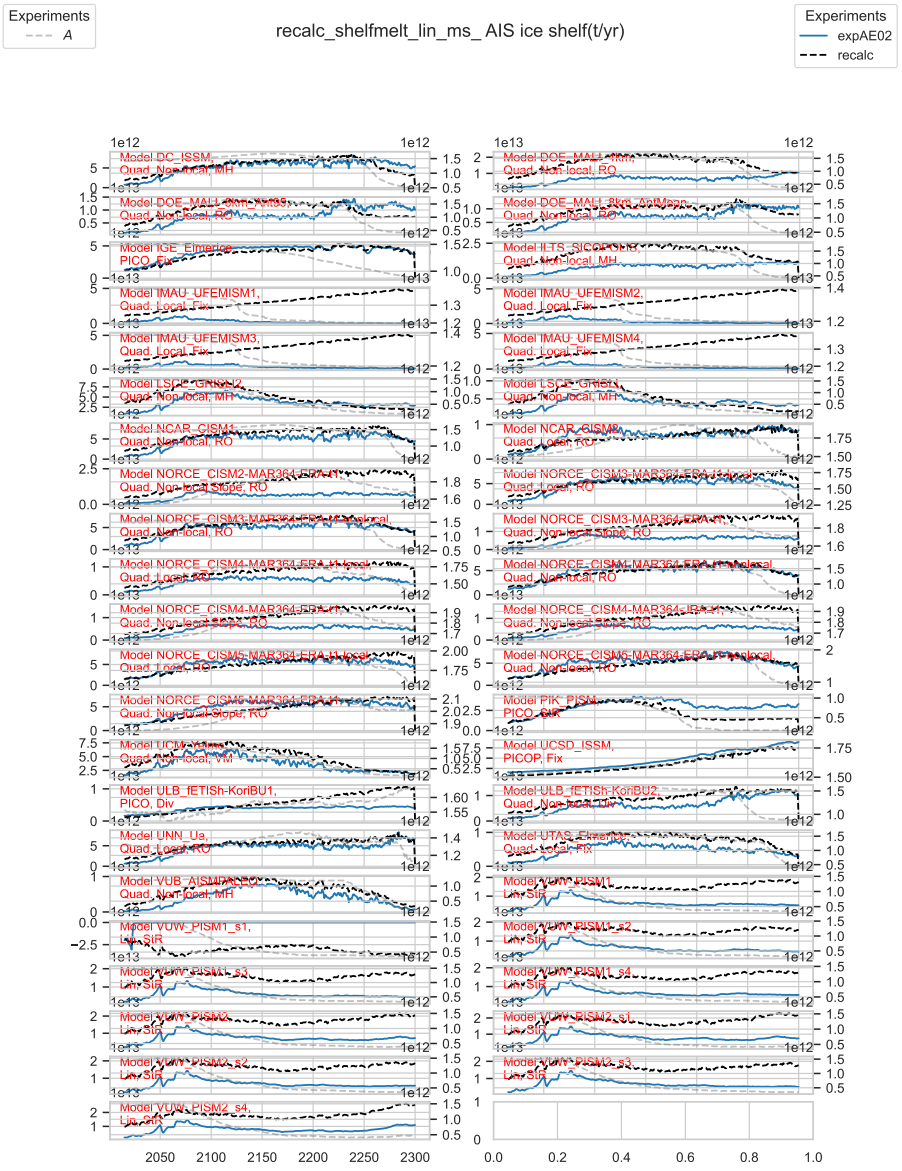

Figure S2. Predicted (dashed black) and actual (blue) BMB evolution for the entire AIS exp02.

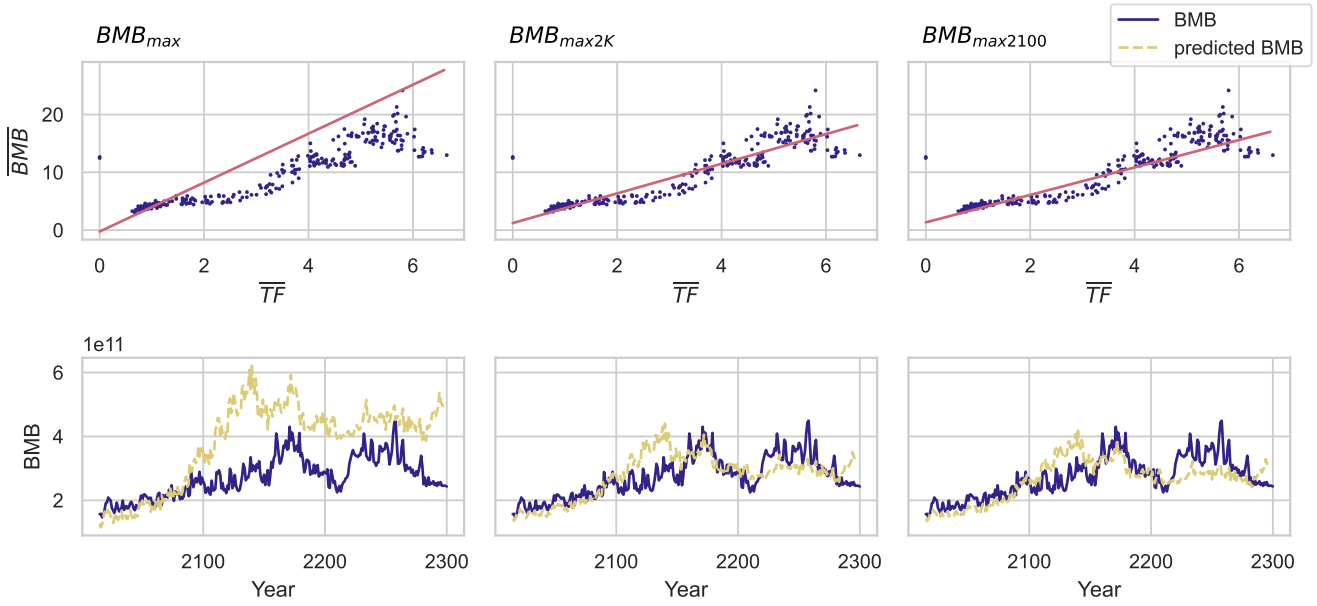

Figure S3. The three fitting strategies to determine the melt sensitivity factor exemplified for the NORCE_CISM5_local model simulation in the Aurora subglacial basin: (i) BMB_{max} fitting prior to the point of maximum basal melt $t = t(\text{BMB\_max})$ in the left-most column; (ii) $\text{BMB}_{\text{max2k}}$ fitting up to the minimum of either the point of maximum basal melt or where the thermal forcing is equal to or less than 2 K, $t = \min(t(\text{BMB\_max}), t(\text{TF} \leq 2K))$ in the middle column; and (iii) $\text{BMB}_{\text{max2300}}$ fitting up to the minimum of either the point of maximum basal melt or 2100, $t = \min(t(\text{BMB\_max}), 2100)$ in the right-most column.

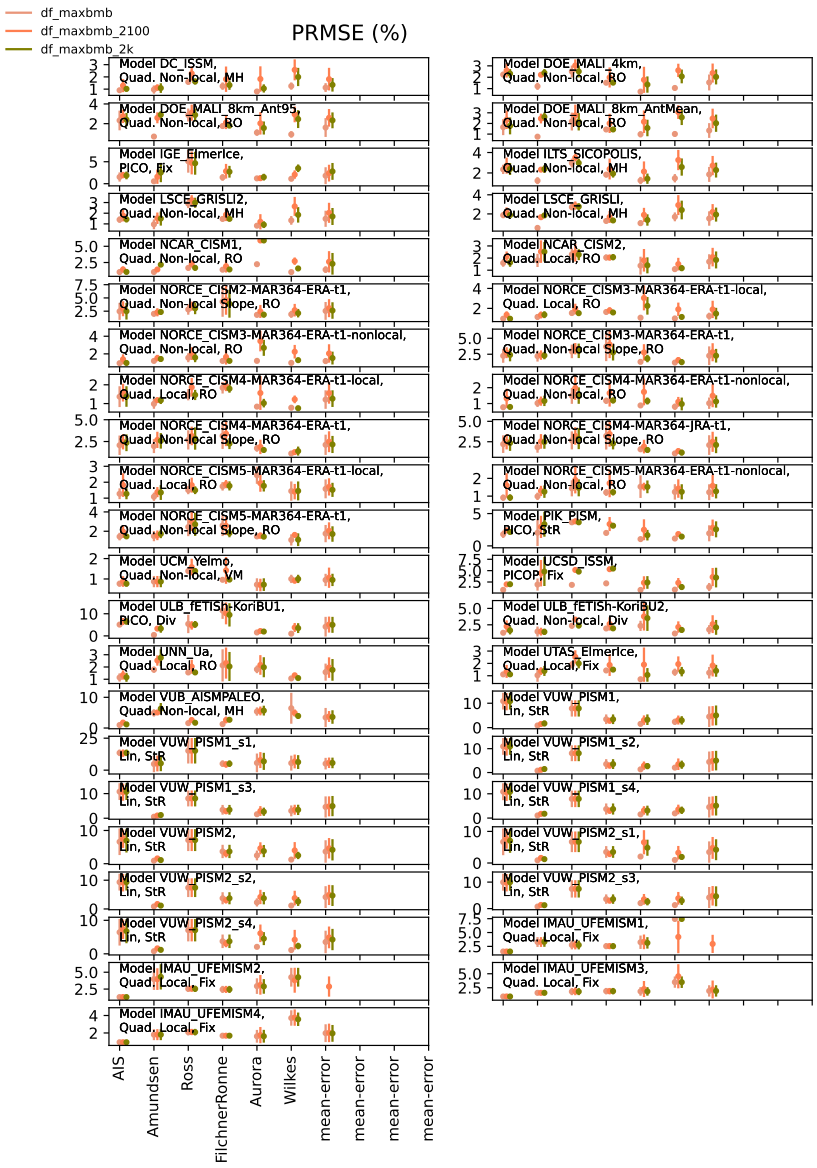

Figure S4. PRMSE for each region and model simulation for the three different MS factor fitting methods.

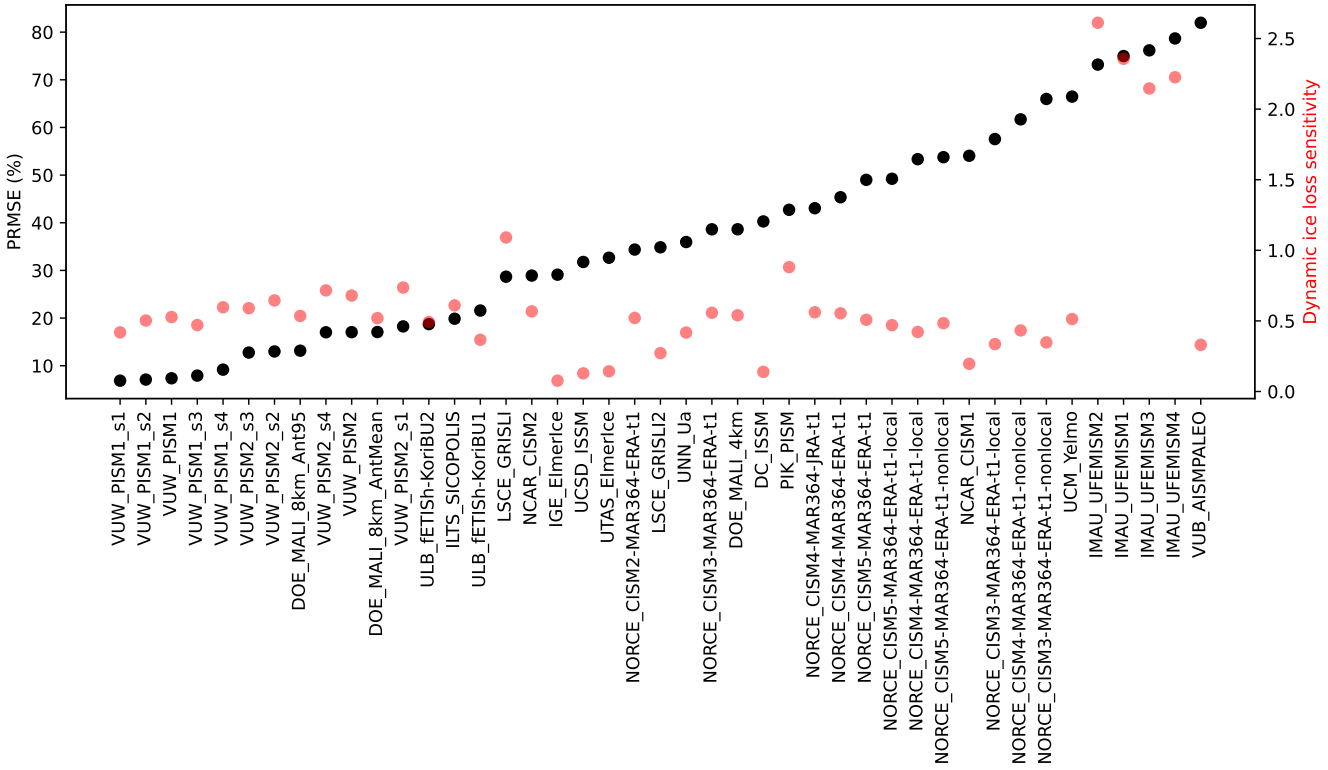

Figure S5. Percentage root mean square errors (PRMSE; %) between the actual and predicted dynamic sea level contribution (black) for the aggregated AIS data, and the corresponding dynamic ice loss sensitivity factors (red). PRMSEs are averaged over the four climate experiments.

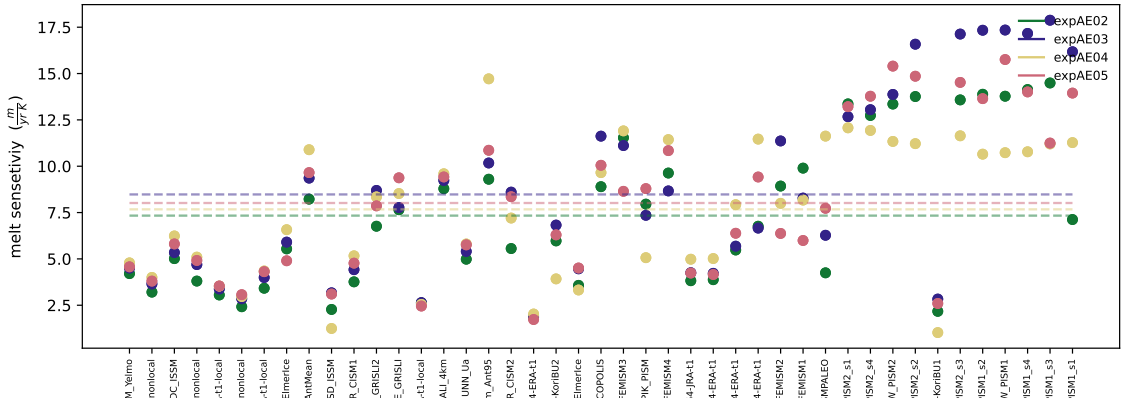

Figure S6. Mean MS factors ($\mathrm{m\,yr^{-1}\,K^{-1}}$) for all regions and ice sheet model simulations. MS factors are coloured by experiment (exp02-exp05). Dashed lines are the mean MS factors across all model simulations, coloured by experiment.

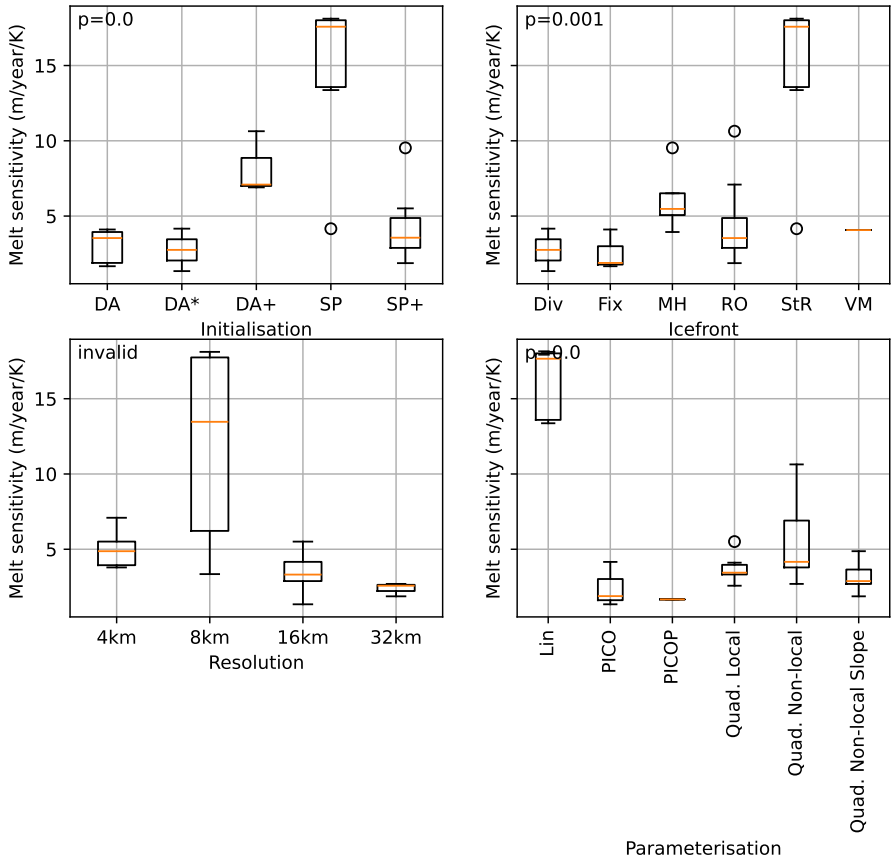

Figure S7. Box plots of the relationship between melt sensitivity factor ($\mathrm{m\,yr^{-1}\,K^{-1}}$) and: initialisation procedure (upper left); icefront calving procedure (upper right); resolution (lower left); and melt rate parameterisation (lower right). Statistical significance (p-value) of the differences in the medians of each group is reported in the upper left corner of each panel, as determined by the Kruskal-Wallis H-test. In each panel, the orange horizontal line is the median, the limits of the box show the interquartile range, the whiskers show data lying with 1.5 times the interquartile range, and circles show outlying data.

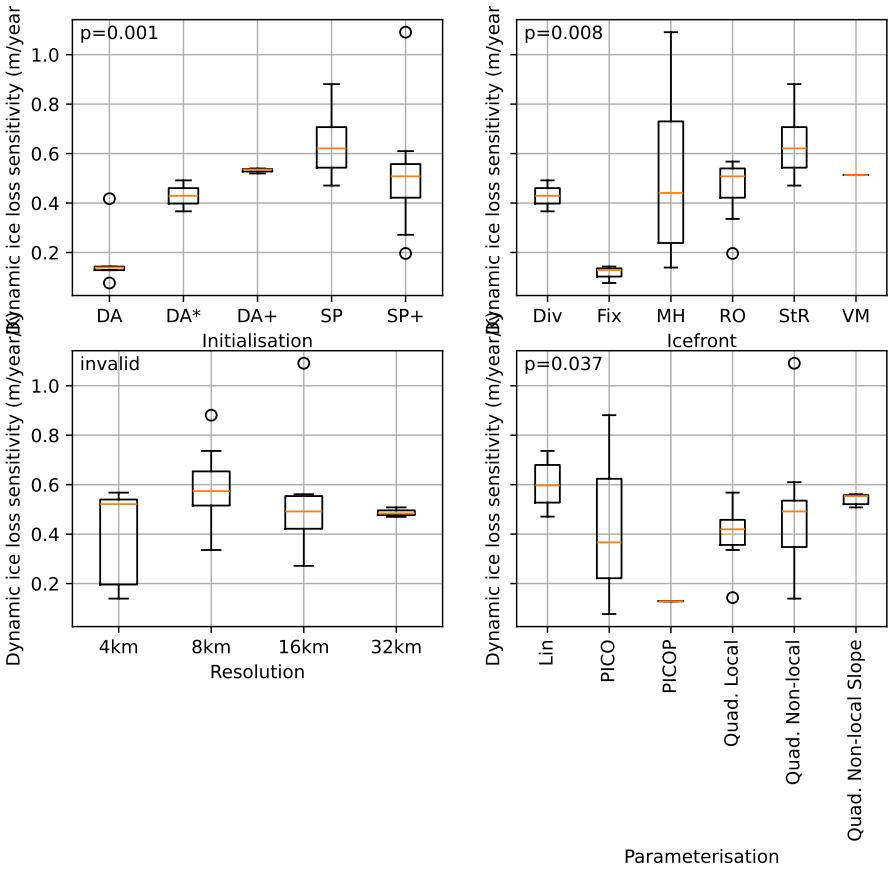

Figure S8. As for figure S7, but for the dynamic ice loss sensitivity factor.

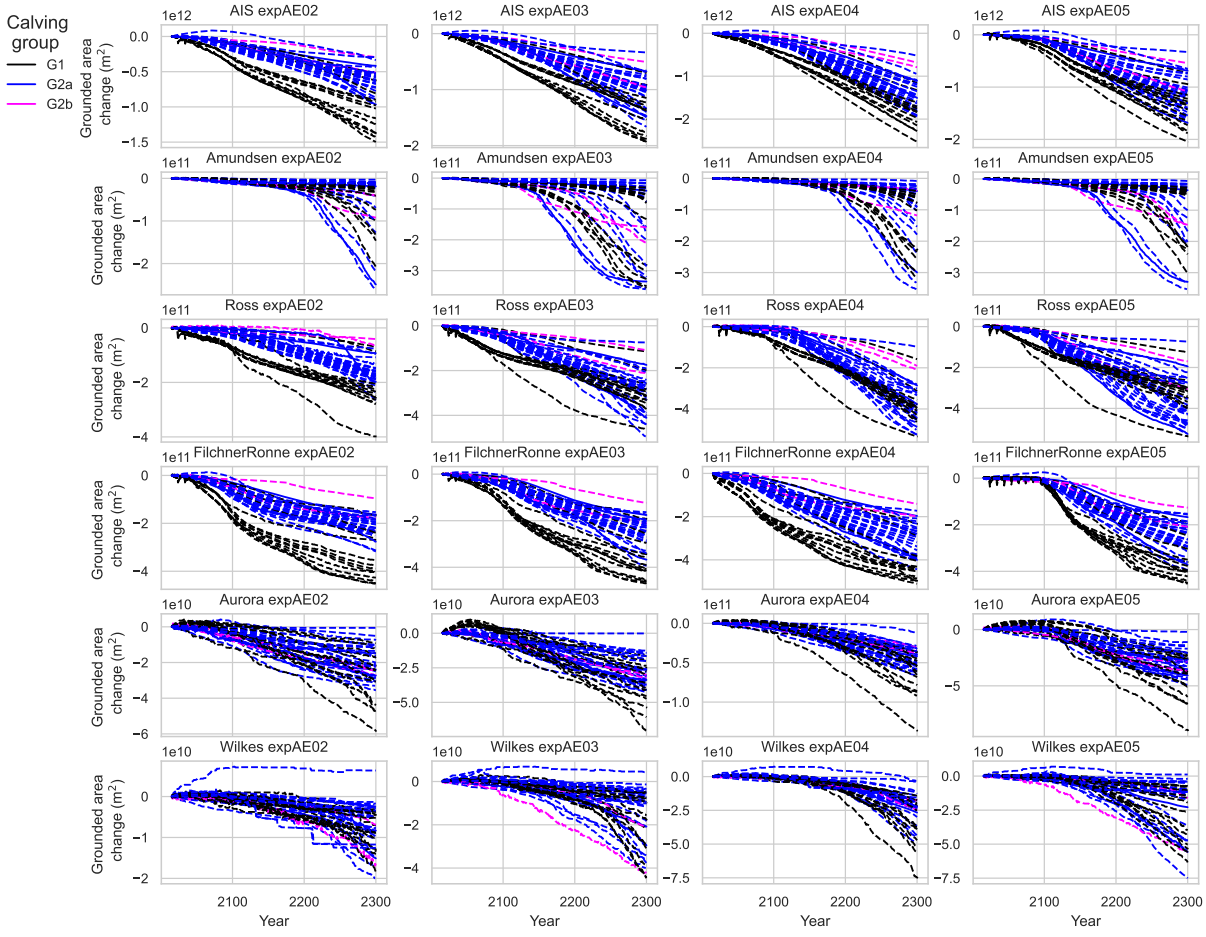

Figure S9. Grounded area changes (m^2) from 2015 to 2300 for different regions of the Antarctic Ice Sheet, including the Amundsen Sea sector, Ross Ice Shelf, Filchner-Ronne Ice Shelf, Aurora Basin, and Wilkes Basin (from top to bottom). Different columns represent results from different experiments (exp02-exp05) from left to right. The colours represent three model groupings: group 1 (black) consists of models with aggressive calving; group 2 (blue) includes models with moderate calving; and group 3 (pink) comprises models with a fixed calving front.

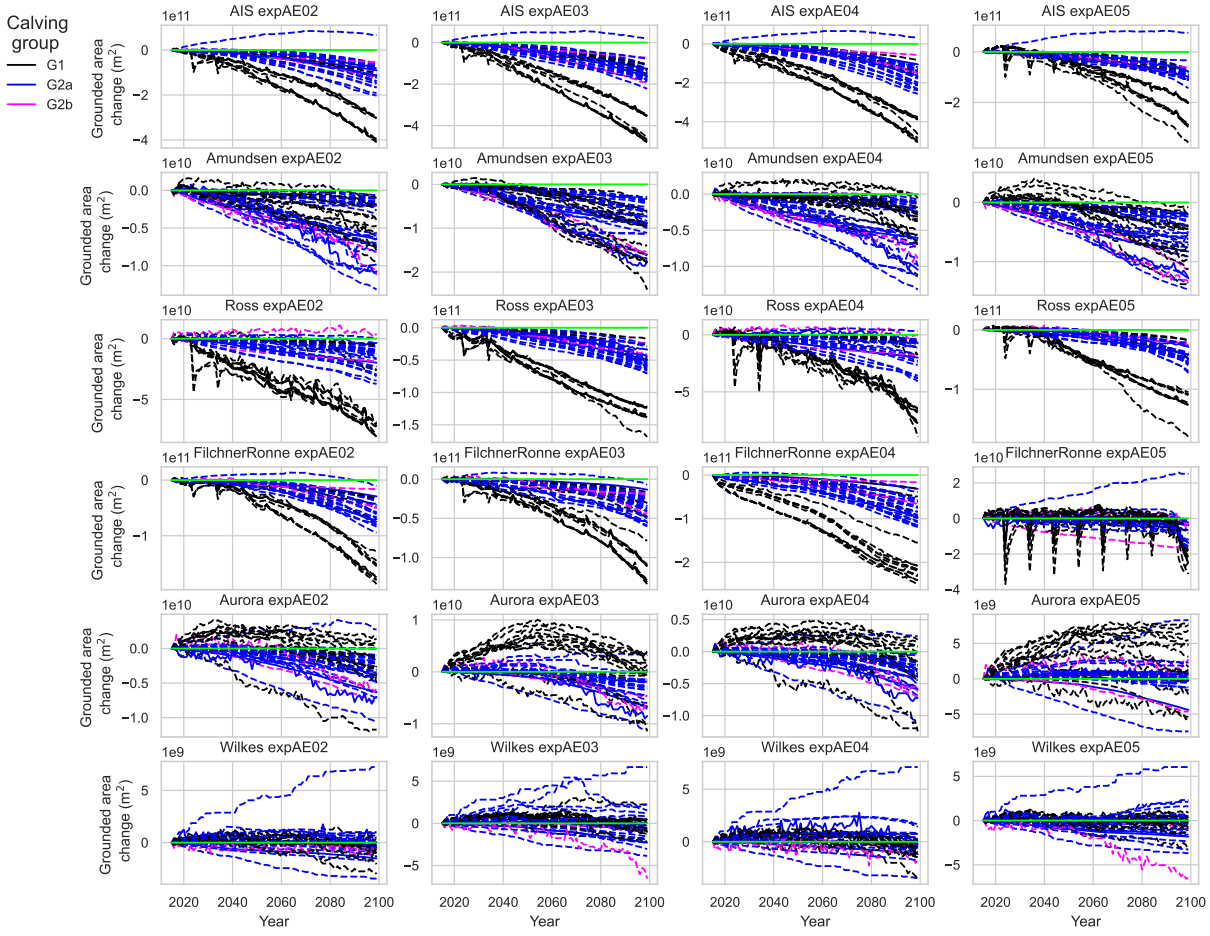

Figure S10. As for figure S7, but to 2100. The green horizontal line represents zero grounded area change.

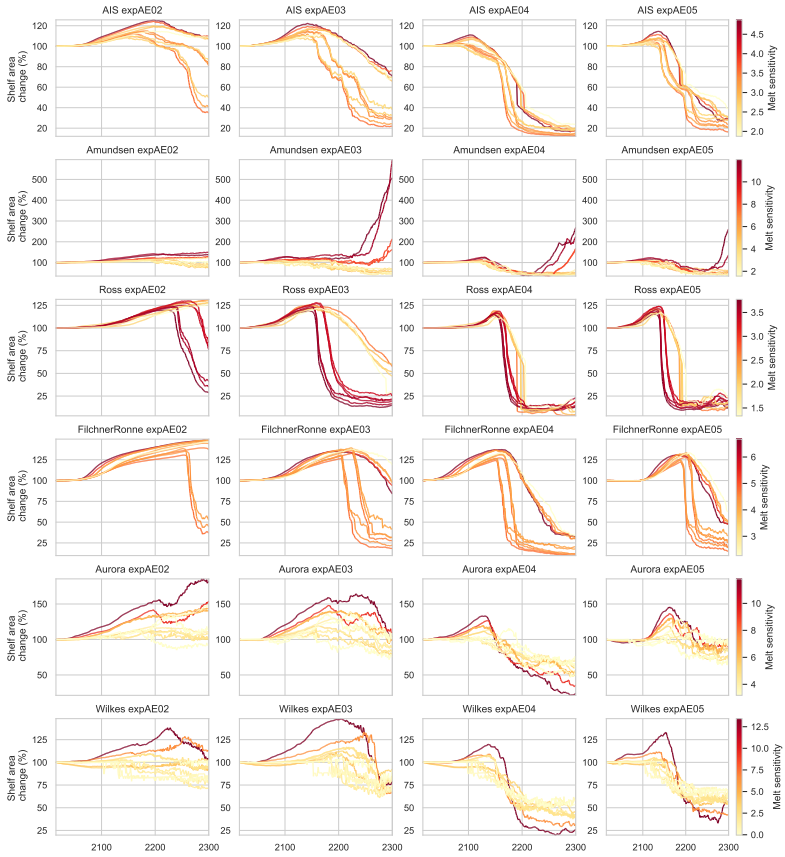

Figure S11. Percentage change in ice shelf area for the NORCE-CISM model ensemble. Colours represent the melt sensitivity factor (red for high melt sensitivity factors; yellow for low melt sensitivity factors).

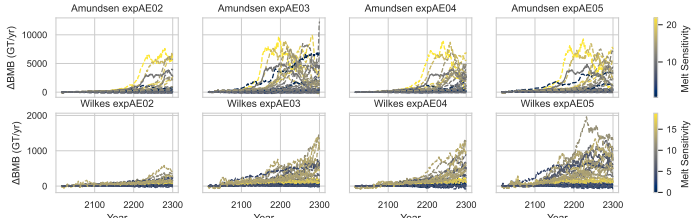

Figure S12. Change in total BMB (Gt/year) in the Amundsen (top row) and Wilkes (bottom row) regions, coloured by MS factors. Columns represent experiments exp02-exp05.

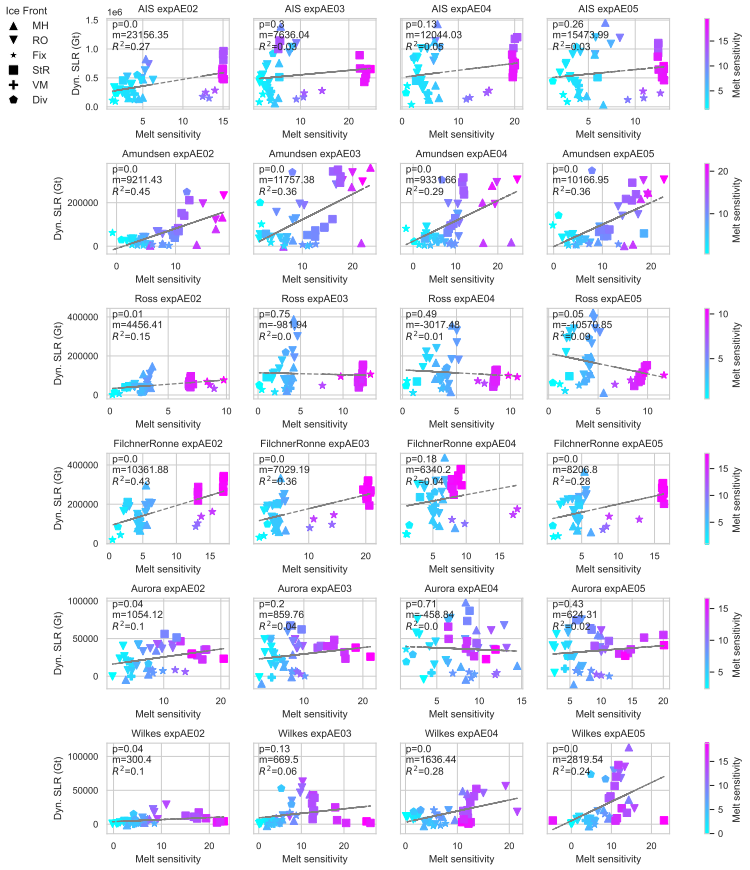

Figure S13. Melt sensitivity ($\mathrm{m\,yr^{-1}\,K^{-1}}$) versus dynamic sea level rise (Gt) at 2300 for different regions of the Antarctic Ice Sheet, including the Amundsen Sea sector, Ross Ice Shelf, Filchner-Ronne Ice Shelf, Aurora Basin, and Wilkes Basin (from top to bottom). Different columns represent results from experiments (exp02-exp05) from left to right. Colours are the best melt sensitivity for each model and region across all experiments. Linear regression line is plotted in gray, with p-values and slope reported in each panel. As per figure 6 of the main manuscript, statistical significance, slope, and coefficient of determination are reported in the top left of each panel (p-, m-, and R^2 values, respectively).

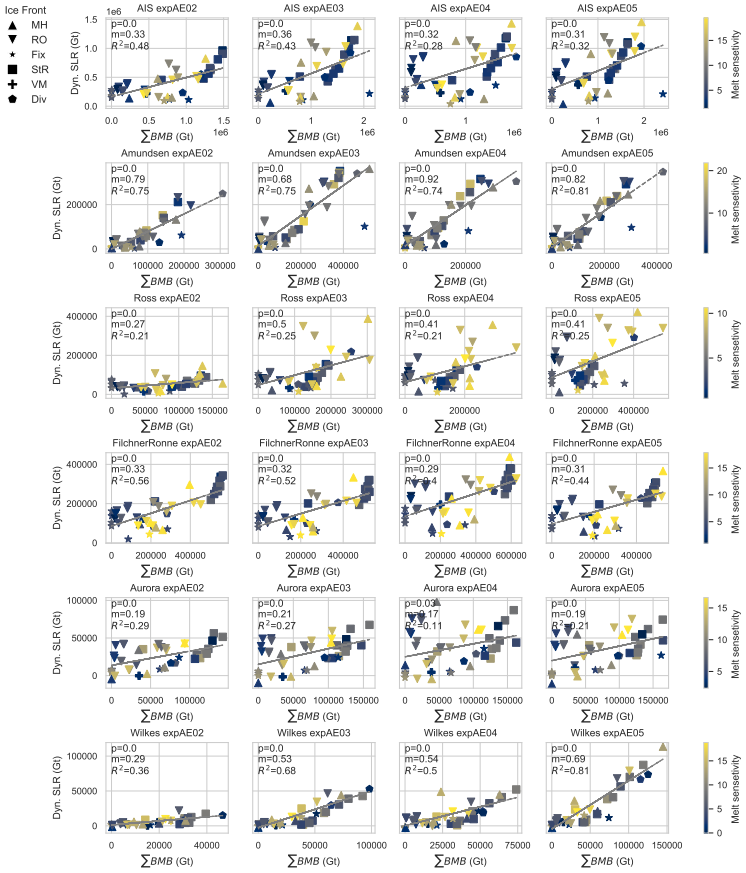

Figure S14. Dynamic sea level rise (Gt) versus total BMB within a 32 km corridor of the grounding line in 2300. Markers indicate the calving procedure and colours represent MS factors. As per figure 6 of the main manuscript, statistical significance, slope, and coefficient of determination are reported in the top left of each panel (p-, m-, and R^2 values, respectively).